Optics & Laser Technology 49 (2013) 86–90

Contents lists available at SciVerse ScienceDirect

Optics & Laser Technology

journal homepage: www.elsevier.com/locate/optlastec

Lidar with SiPM: Some capabilities and limitations in real environment

Ravil Agishev [a,c,*], Adolfo Comerón [a], Jordi Bach [a], Alejandro Rodriguez [a], Michaël Sicard [a], Jordi Riu [b], Santiago Royo [b]

[a] Dept. of Signal Theory & Communications, Universitat Politècnica de Catalunya, Jordi Girona 1-3, 08034 Barcelona, Spain
[b] Center for Sensors, Instrumentation & Systems Development, Universitat Politècnica de Catalunya, Rambla Sant Nebridi 10, 08222 Terrassa, Spain
[c] Kazan National Research Technical University, 10, K. Marx St., Kazan 420111, Russian Federation

ARTICLE INFO

Article history:
Received 24 October 2012
Received in revised form
15 December 2012
Accepted 18 December 2012
Available online 23 January 2013

Keywords:
Lidar
SiPM
PMT

ABSTRACT

The purpose of the work is to demonstrate real capabilities and to give examples of SiPMs application in lidar technology in both analog and photon counting modes. The experimental research within an operating lidar complex adapted to implement the analog mode and photon counting measurements with subsequent inversions of atmospheric extinction and backscattering coefficients was conducted. Theoretical evaluations of potential limitations of atmospheric lidar by use of real day-time background parameters and features of SiPM-photodetectors studied experimentally were carried out with comparison of the extent of sensitivity decreasing for different detectors used and estimations of their operation range reduction.

1. Introduction

Laser remote sensing technology using lidars as instruments of environmental monitoring intensively developed and successfully applied in various fields [1–5]. The lidar systems belong to a wider class of location systems [3,4,6,7], but the lidars operation conditions and requirements to them have a number of basic features which make an impact on their design and operation. The most important features among them are the followings: a wide dynamic range of echo-signals received; low level of optical signals coming from the scattering medium depth; high intensity of background radiation at daytime operation of lidar.

In the past few years, research groups in different countries actively developed the SiPM (silicon photomultiplier) detectors, which expand traditional applications of high-sensitivity photodetectors on PMTs and APDs (photomultipliers and avalanche photodiodes) and demonstrated new properties that were previously unattainable [8,9]. At the same time, we know the only paper [10] devoted to SiPMs in analog mode used in atmospheric lidars, although the prospects for their application in lidars seem to be very wide.

One of purposes of the paper is to demonstrate real capabilities and to give examples of SiPMs introduction into lidar technology with detecting signals in both analog and photon counting modes. At the same time, when using any type of high-sensitivity photodetectors, an intense sky background reduces the measurements accuracy, limits the operation range that reduces the lidar's range of measurement conversion (from optical input to electrical output), thus reducing the lidar system potential. Moreover, under intense daytime sky background the traditional methods of spectral, spatial and temporal selection of signals are not sufficiently effective to achieve the required values of signal-to-noise ratio [2,4,5]. In some cases, the strong background radiation can saturate and overload the photodetector.

The conventional approach to analyze the relation between lidar echo-signals, external backgrounds and internal noise is based on the use of rigorous models of photodetectors [3,4,7]. This requires taking into account a large number of specific component parameters for different lidar photodetectors. At the same time, basing on their detailed and well-grounded approaches, the lidar signal-to-noise ratio can be presented in a simple and translucent form as follows:

$$\rho = P_s / \sqrt{P_q(P_s + P_b) + P_n{}^2} \tag{1}$$

where P_s is the received lidar signal power; P_b is the sky background radiation power; P_n is the internal noise power of the photodetector normalized to the input. In turn, $P_q = 2 \cdot h \cdot c \cdot F \cdot \Delta f / \lambda \cdot \eta$, and $P_n = \mathrm{NEP} \cdot \Delta f^{1/2}$, where h is the Planck's constant; c is the light velocity; F is the coefficient of noise magnification during internal amplification (i.e., an excess noise factor); Δf is the receiver transmission band; λ is the wavelength; η is the quantum efficiency of the photodetector; NEP (noise equivalent power) is the equivalent

* Corresponding author at: Kazan National Research Technical University, 10, K.Marx St., Kazan 420111, Russian Federation. Tel.: +7 843 2310244.
E-mail address: ravil_agishev@mail.ru (R. Agishev).

0030-3992/$ - see front matter © 2012 Elsevier Ltd. All rights reserved.
http://dx.doi.org/10.1016/j.optlastec.2012.12.024

power of internal noise of the photodetector independent of signal and background, per unit of frequency.

When the receiver's sensitivity limits by the quantum noise, what often takes place in lidar systems, the quantum noise power P_q provides a useful scale to estimate the power levels of signal, background and internal noise, since they all depend on the same factor of excess noise F, transmission band Δf, wavelength λ, and quantum efficiency η.

Defining the normalized parameters as $\Psi_s \equiv P_s/P_q$, $\Psi_b \equiv P_b/P_q$, $\Psi_n \equiv P_n/P_q$, the different operating regimes expressed by the Ψ-values, can be determined: from weak values: $\Psi << 1$ to strong ones: $\Psi >> 1$. Then Eq. (1) can be rewritten as [12]

$$\rho^2 = \Psi_s^2 / \left(\Psi_s + \Psi_b + \Psi_n^2\right) \tag{2}$$

The quadratic equation for Ψ_s can be written as

$$\Psi_s^2 - \rho^2 \Psi_s - \rho^2\left(\Psi_b + \Psi_n^2\right) = 0,$$

and the normalized threshold signal power P_t/P_q for a given S/N level ρ will be

$$\Psi_s^{\min} \equiv P_t/P_q = 1/2\ \rho^2\left(1 + \sqrt{1 + 4\left(\Psi_b + \Psi_n^2\right)/\rho^2}\right)$$

By introducing the dimensionless parameter U_b as the ratio of photodetector threshold powers P_t^B and P_t^0:

$$U_b \equiv \frac{P_t^B}{P_t^0} = \frac{\Psi_s^{\min}}{\Psi_s^{\min}(\Psi_b = 0)},$$

which are obtained in presence (B) and absence ($B=0$) of the background noise:

$$U_b = \left[1 + \sqrt{1 + \frac{4}{\rho^2}\Psi_n^2\left(1 + \frac{\Psi_b}{\Psi_n^2}\right)}\right] \Big/ \left(1 + \sqrt{1 + \frac{4}{\rho^2}\Psi_n^2}\right) \tag{3}$$

it is easy to assess quantitatively an extent of the lidar performance degradation. Namely, for any lidar type and configuration, on the basis of U_b we can compare the extents of sensitivity decreasing for different detectors used and then we can obtain the operation range reduction.

The above given expressions and their further development can be used to give a measure to further applicability of experimental results, obtained with use of a setup adapted to implement the analog mode and photon counting measurements. Such an experimental setup was developed and mounted as a part of multichannel complex for atmosphere studies on the base of operational lidar. Evaluations of SiPM-lidar limitations with comparison of sensitivity decreasing for different photodetectors we used and with estimations of the operation range reduction under intense background noise are indicative to predict the potential of SiPM-lidars based on comparison of both experimental and theoretical approaches which complement each other.

2. Experimental studies

Experimental studies and measurements based on previously conducted specialized engineering designs and adapted to implement the analog mode and photon counting measurements were carried out in the specialized laboratory on the basis of the UPC (Universitat Politècnica de Catalunya) lidar, which is actively used in several European and Spanish R&D programs. Lidar represents a 6-channel automated laser-based measuring complex for atmospheric optical research [11].

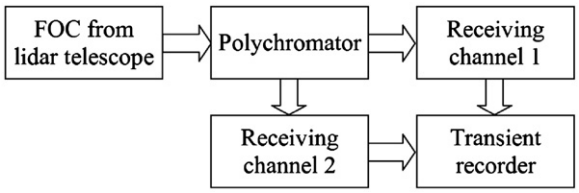

Fig. 1. Experimental setup within operating lidar system.

2.1. Experimental setup and lidar signals

To experimentally assess the feasibility of new SiPM-detectors as a part of this lidar complex, we used a 2-channel polychromator. As detectors the SensL 30035 (hereinafter SiPM-S) and the Hamamatsu S10362-33-100C (SiPM-H) were used. Together with the final transimpedance amplifier they were turn-based built into the 1st channel of the polychromator. To compare the features of two SiPM-detectors, in the 2nd channel of the polychromator we used the PMT Hamamatsu R7400P (PMT-H), which is widely used in atmospheric lidars.Fig. 1

As an example, the lidar signals from the SiPM-S detector are presented in analog and photon counting modes in Fig. 2. For comparison, the signal from the PMT-H is shown. These waveforms were selected from a set of regular lidar measurements performed at UPC.

2.2. Primary processing of measurement results

In Figs. 3, 4 we show the initial processing results of automated lidar measurements using turn-based SiPM-S or SiPM-H in the 1st channel and with the PMT-H in the 2nd channel. Fig. 3 includes: (1) a color illustration of range-square (R^2) corrected optical weather changes for 10 min. integration period; (2) the backscatter coefficient profiles retrieved from the lidar signal on a 0–6 km path; (3) the same retrieved signal on a 0.5–1.5 km path. In Fig. 3, the selected R^2-corrected lidar signal profiles and the time-averaged profile corresponding to the same first cloud are shown.

Fig. 4 shows the time series of range-square-corrected lidar signals and the retrieved range profile of the atmospheric extinction coefficient. They were obtained when using the SiPM-H detector in analog detection and photon counting modes as well as using the PMT-H for comparison.

As it is seen from Figs. 2–4, the measurements carried out by use of the SiPM-S and SiPM-H detectors and their initial processing results are very well correlated with those obtained by the commonly used PMTs.

3. How the obtained experimental results can be used. Evaluation of the potential and limitations inherent to lidars with SiPMs

3.1. Further use of U_b-parameter

For considered silicon photomultipliers SiPMs and traditional photomultiplier tubes PMT under inequalities the following inequalities are satisfied:

$P_b >> P_q >> P_n$ or $\Psi_b >> 1 >> \Psi_n$,

Then one can obtain from Exp. (3) the following relation at $\rho = 1$:

$$U_b \approx \sqrt{\Psi_b} = \sqrt{\lambda/2hc\Delta f} \times \sqrt{P_b} \times \sqrt{\eta(\lambda)/F} \tag{4}$$

This is an expression to predict the lidar sensitivity reduction under intense background radiation for different photodetectors.

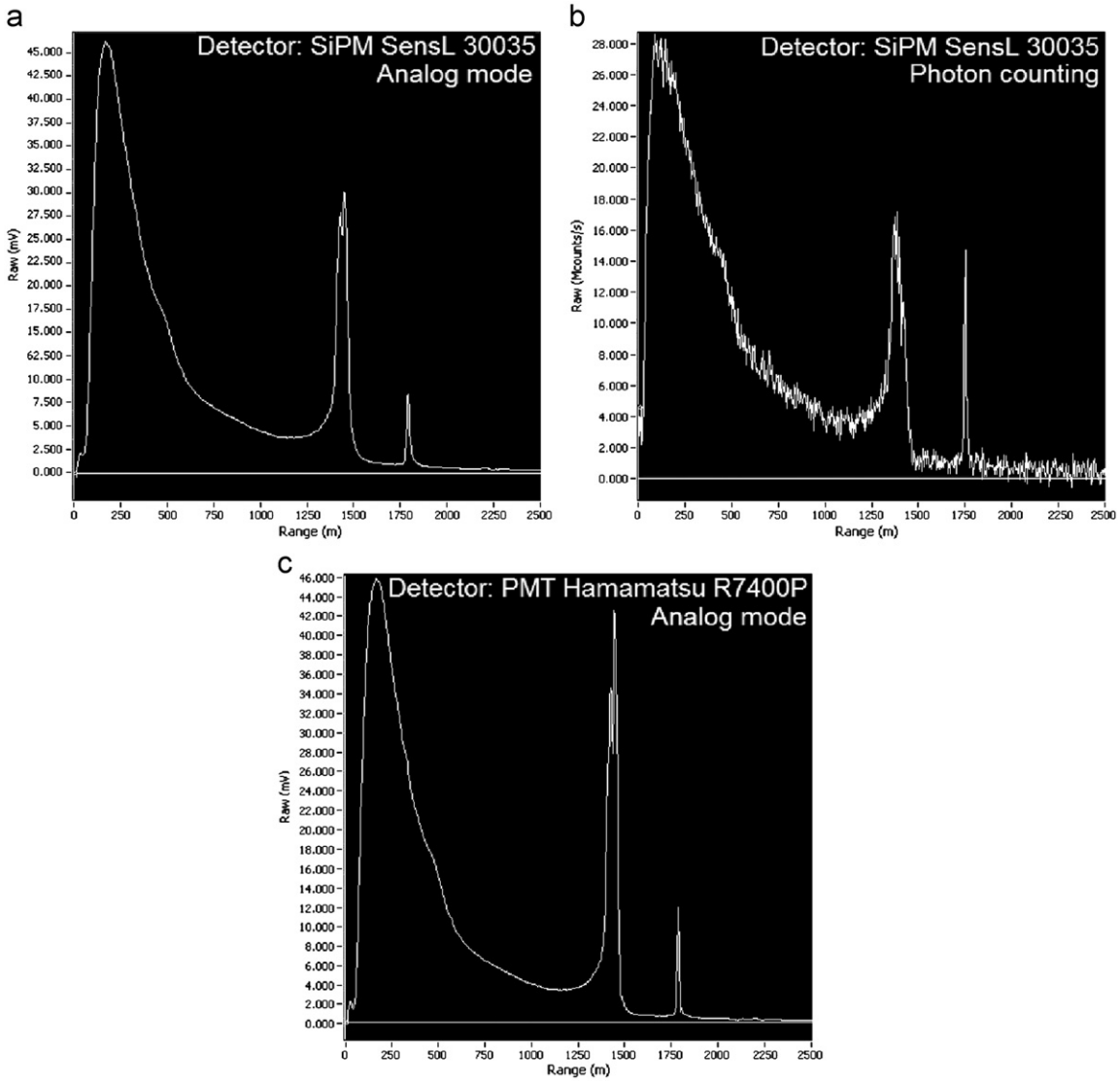

Fig. 2. Lidar signals with SiPM-detector SensL 30035 in the analog (a) and photon counting (b) modes. For comparison: PMT Hamamatsu R7400P in the analog mode (c).

To describe specific features of SiPMs which have been studied experimentally in Section 2, only two their specific characteristics are needed, namely: the photon detection efficiency (PDE) $\eta(\lambda)$ and the excess noise factor F. To compare them with PMT-detectors which traditionally used in lidar, we use the generalized model of PMT that was earlier introduced in our paper [12, Section 4.1 and Fig. 5].

In Fig. 5, the $\eta(\lambda)$ curves of the earlier experimentally studied SiPMs, namely the SiPMs SensL 30035 and SiPMs Hamamatsu S10362-33-100C are presented; the $\eta(\lambda)$curves of $PMT_{generalized}$ are given as well. The F coefficients for all photodetectors mentioned are considered equal to 1.30/1.42/1.20 correspondingly.

The normalized curves $U_b/P_b^{1/2}(\lambda)$ for lidar with SiPM-S/ SiPM-H/ $PMT_{generalized}$ detectors are shown on the same Fig. 5. The quantitative estimation of the threshold sensitivity decreasing can be obtained, if to multiply any $U_b/P_b^{1/2}(\lambda)$ value from Fig. 5 by the actual value of $P_b^{1/2}$ related to the current sky background power.

3.2. Reduction of operating range under intense background

To estimate the reduction of the lidar operating range under intense sky background, the echo-signal power P_s can be written as $\Psi_s \equiv P_s/P_q = A/R^2P_q$ (A is the proportionality coefficient), if for simplification we neglect the signal extinction in a relatively transparent atmosphere in relatively transparent atmosphere with the optical density $\tau = \alpha R < 1$ (α is the atmospheric extinction) and take into account only its geometrical extinction that is proportional to a range squared. Therefore, Eq. (2) has the form:

$$\rho^2 = A^2/\{R^4P_q^2[A/\left(R^2P_q\right) + \Psi_b + \Psi_n^2]\}$$

Then it is easy to obtain an expression for reduction of lidar operating range under intense background, when the lidar operation range under background radiation $R_{B\ \max}$

$$R_{B\max}^2 = \frac{A}{2\left(\Psi_b + \Psi_n^2\right)P_q}\left[\sqrt{1 + \frac{4\left(\Psi_b + \Psi_n^2\right)}{\rho^2}} - 1\right]$$

and without background $R_{0\max}$:

$$R_{0\max}^2 = -\frac{AP_q}{2\Psi_n^2P_q^2} + \frac{\sqrt{A^2P_q^2 + 4\Psi_n^2P_q^2\left(A^2/\rho^2\right)}}{2\left(\Psi_b + \Psi_n^2\right)P_q^2}$$

$$= \frac{A}{2\Psi_n^2P_q}\left[\sqrt{1 + \frac{4\Psi_n^2}{\rho^2}} - 1\right]$$

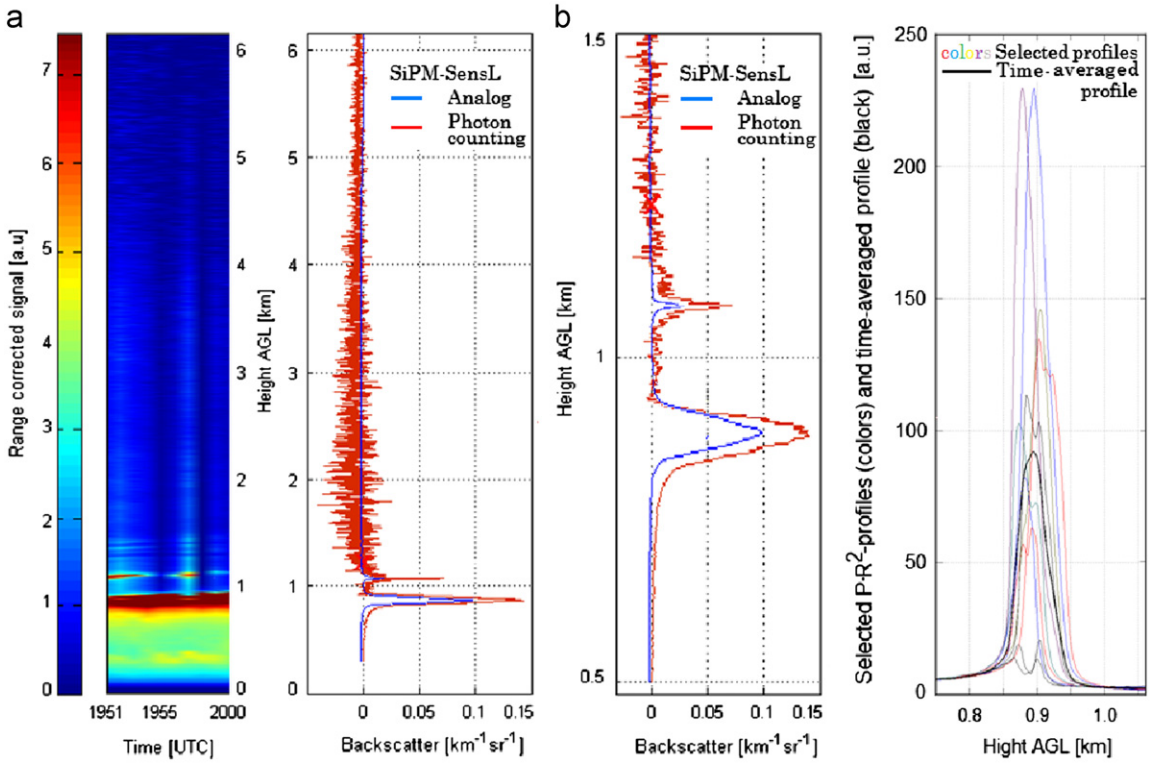

Fig. 3. (a) R^2-corrected lidar signals' time series (left) and backscattering coefficient inversions (mid and right) with SiPM-SensL in analog (blue) and photon counting (red) modes; (b) selected (colors) and time-averaged (black) R^2-compensated profiles from the same first cloud. (For interpretation of the references to color in this figure legend, the reader is referred to the web version of this article.)

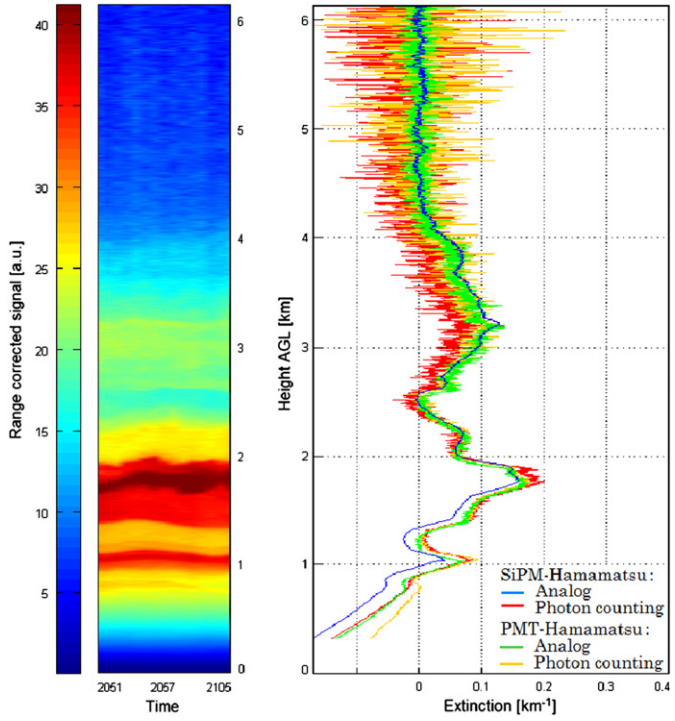

Fig. 4. The R^2-corrected signals' time series and atmospheric extinction coefficient profiles obtained from the SiPM-Hamamatsu signals in analog (blue) and photon counting (red) modes. For comparison: the same for the PMT Hamamatsu (green and yellow). (For interpretation of the references to color in this figure legend, the reader is referred to the web version of this article.)

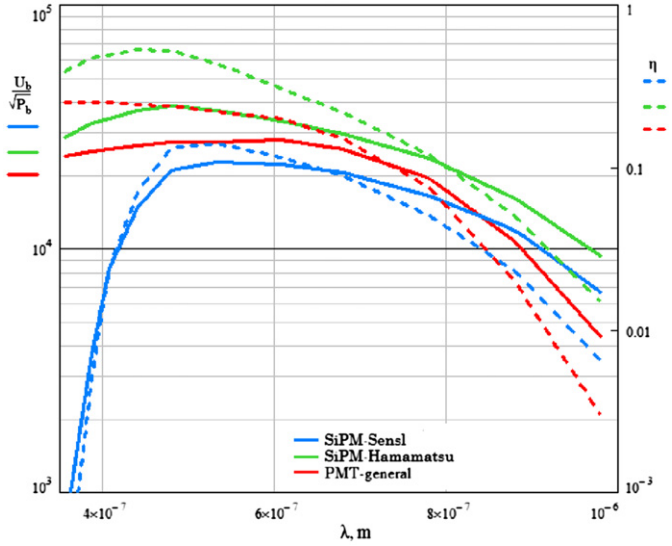

Fig. 5. Spectral dependences of normalized threshold sensitivity $U_b/P_b^{1/2}(\lambda)$ and photon detection efficiency $\eta(\lambda)$ of different lidar detectors.

are determined as follows:

$$r_b \equiv \frac{R_{B\max}}{R_{0\max}} = \sqrt{\left[\sqrt{1+\frac{4}{\rho^2}\Psi_n^2\left(1+\frac{\Psi_b}{\Psi_n^2}\right)}-1\right] \Big/ \left[\left(1+\frac{\Psi_b}{\Psi_n^2}\right)\left(\sqrt{1+\frac{4}{\rho^2}\Psi_n^2}-1\right)\right]} \tag{5}$$

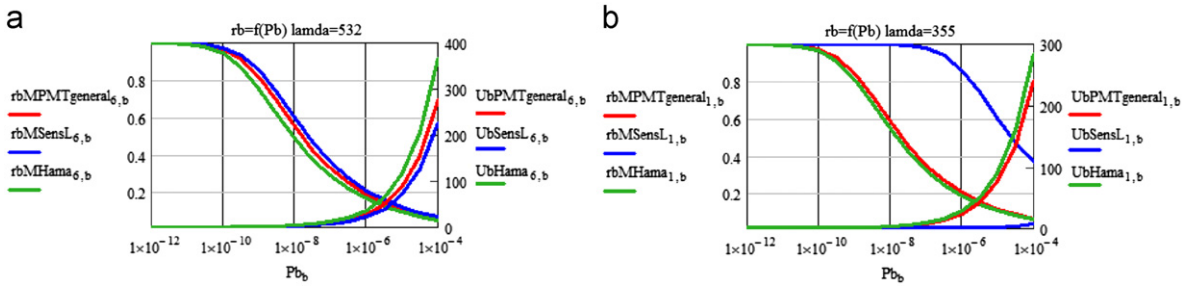

Fig. 6. Reduction of normalized operation range r_b and of U_b-parameter under intense background radiation P_b at $\lambda=532$ nm (a) and 355 nm (b).

3.3. Interpretation of modeling results

Taking into account that the inequalities $P_b >> P_q >> P_n$ are satisfied for SiPMs and PMTs considered (although the right-hand inequality is satisfied much stronger for PMTs) and by using the U_b-parameter from Exp. (3), the reduction in the lidar operation range can be compactly written as:

$$r_b = U_b{}^{-1/2} \tag{6}$$

Of course, other atmospheric affects would complicate the analysis of relations between r_b and U_b.

From Exp. (6) another physical interpretation of the system parameter U_b becomes clear: its inverted numerical value defines a square of a normalized operation range of lidar, when taking into account only the geometrical extinction of the echo-signal in relatively transparent atmosphere with $\tau=\alpha\ R<1$.

By using details from Exp. (4) and for $\rho=1$, we can rewrite Eq. (6) as follows:

$$r_b = \frac{\sqrt[4]{2hc\Delta fF/\lambda\eta(\lambda)}}{\sqrt[4]{P_b}} = \sqrt[4]{P_q/P_b} \tag{7}$$

or

$$r_b P_b^{1/4} = P_q^{1/4} \tag{8}$$

From Eq. (7), the operation range reduction for a day-time working lidar can be easily assessed for detector with specific features of $\eta(\lambda)$ and F in lidar system with operation λ and Δf, if the sky background power P_b is measured or properly estimated. By applying above mentioned assessments to silicon photodetectors SiPMs under consideration, the results shown in Fig. 6 can be obtained.

As it is seen from Exps. (7) and (8), for any lidar a value of the $r_b P_b^{1/4}$ product is a constant equal to $P_q^{1/4}$. In other words, the fourth root of the photodetector's quantum noise power P_q cannot be exceeded. This means, for example, that the Hamamatsu SiPMs with the less P_q value than SensL SiPM- and PMT- photodetectors due to much less value of the F/η ratio, will always have less operation range r_b than the SensL SiPMs and PMTs at the same external background power P_b. In turn, one can observe the clourable advantage of the SensL SiPMs (blue color) at 355 nm, which is determined by their considerably worse quantum efficiency at the UV wavelengths.

4. Conclusions

In the paper presented, we have demonstrated real capabilities of SiPMs introduction into lidar technology. We have conducted a set of measurements with SiPM-Hamamatsu and SiPM-SensL detectors on the specialized experimental setup on the base of operational lidar by detecting signals in both analog and photon counting modes and by subsequent obtaining inversions of atmospheric extinction and backscattering coefficients. Theoretical evaluations of SiPM-lidar limitations closely connected with experimental studies were carried out. By use of parameters of a real day-time background and features of SiPM-photodetectors, the lidar sensitivity reduction caused by background radiation for different photodetectors was compared and the related operation range reduction was estimated. This allows researchers to give a measure for further applicability of experimental results obtained at the current level of SiPMs production technology.

Acknowledgements

The authors thank the Spanish Ministry of Science and Innovation (MICINN) for projects DPI2009-13379, and DPI2011-25525, which partially funded this research. The lidar activities are supported by the EU's 7th FP project Aerosols, Clouds, and Trace Gases Research Infrastructure Network (ACTRIS), Grant agreement 262254, and by the MICINN and FEDER funds under the project TEC2009-09106/TEC, and the Complementary Actions CGL2009-08031-E/CLI, CGL2010-09225-E, CGL-2011-13580-E/CLI, and CGL2011-16124-E/CLI.

References

[1] Measures R. Laser remote sensing: fundamentals and applications. New York: Wiley; 1994.
[2] Weitkamp C. Berlin: Springer; 2005.
[3] Osche G. Optical detection theory for laser applications. New York: Wiley; 2002.
[4] Minkoff J. Signal processing fundamentals and applications for communications and sensing systems. Norwood: Artech House; 2002.
[5] Agishev R. Lidar monitoring of the atmosphere. Moscow: PhysMathLit Press; 2009.
[6] Jelalian A. Laser radar systems. New York: Artech House; 1992.
[7] Keiser G. Optical fiber communication. NY: McGraw-Hill; 2000.
[8] G Barbarino, R de Asmundis, G de Rosa, Silicon photo multipliers detectors operating in Geiger regime, in: Photodiodes—World Activities in 2011, J.-W.Park (editor), In TechOpen, 2011, pp.183–226.
[9] Del Guerra A, Belcari N, Bisogni M, Corsi F. Silicon photomultipliers as novel photodetectors for PET. Nuclear Instruments and Methods in Physics Research 2011;A648:232–5.
[10] Riu J, Sicard M, Royo S, Comerón A. Silicon photomultiplier detector for atmospheric lidar applications. Optics Letters 2012;37(7):1229–31.
[11] Kumar D, Rocadenbosch F, Sicard M, Comerón A, Muñoz C, Lange D, et al. Six-channel polychromator design and implementation for the UPC elastic/Raman LIDAR. Proceedings of SPIE 2011;8182 pp. 81820W-1-10.
[12] Agishev R, Gross B, Moshary F, Gilerson A, Ahmed S. Simple approach to predict APD/PMT lidar detector performance under sky background using dimensionless parameterization/. Optics and Lasers in Engineering 2006;44(8):779–96.